Annealing of metastable defects in hydrogenated amorphous silicon

M. Stutzmann, W. B. Jackson, and C. C. Tsai
Xerox Corporation, Palo Alto Research Center, Palo Alto, California 94304
(Received 26 August 1985)

The annealing process of light-induced metastable dangling-bond states in hydrogenated amorphous silicon is studied using the analysis presented in the preceding paper for electron-spin-resonance transients. The annealing kinetics are monomolecular, with a thermally activated decay rate $R=\nu_0\exp(-E_a/kT_A)$. The decay curves of the metastable defects in pure, UHV-deposited *a*-Si:H and in *a*-Si:N,H *a*-Si:C,H and *a*-Si:O,H with impurity contents between 1 and 20 at. % are analyzed in terms of a well-defined prefactor, ν_0, and a broad distribution of thermal activation energies, $N(E_a)$. Both ν_0 and $N(E_a)$, depend in a characteristic way on the density and the chemical nature of the impurities present in a sample. Moreover, a strong correlation between ν_0 and $N(E_a)$ similar to the Meyer-Neldel rule for the conductivity in *a*-Si:H is observed. Implications of the experimental results for the intrinsic or extrinsic nature of the metastable defects and possible annealing mechanisms are discussed.

INTRODUCTION

In the preceding paper we developed a method to analyze electron-spin-resonance (ESR) decay transients in terms of paramagnetic defect distributions.[1] This method makes use of the twofold spectroscopic information gained by an analysis of electron-spin-resonance (ESR) transients. In this method, conventional ESR is used to tag a paramagnetic defect of interest. Then, variations in the observed ESR spin density due to generation and/or annealing of the tagged defect can be used to obtain further information about important structural parameters governing the time dependence of the defect density, such as tunneling distances, attempt-to-escape frequencies, and thermal activation energies. In this paper we will apply this analysis to silicon dangling bonds, Si_3^0, which play a central role in the electronic properties of hydrogenated amorphous silicon (*a*-Si:H), an amorphous semiconductor currently used as the electronically active material for large area photoreceptors and thin-film transistor arrays. It is well known that metastable silicon dangling bonds can be created by prolonged illumination of device quality *a*-Si:H. The creation of this defect is thought to occur via recombination-induced breaking of weak (strained) Si—Si bonds, promoted by the large mechanical stresses known to exist in thin-film *a*-Si:H samples and by the presence of large densities of impurities.[2–4]

An important property of these light-induced silicon dangling bonds is their metastable character. By annealing an illuminated sample at temperatures above typically 100 °C, the electronic properties of the sample prior to illumination can be restored within a one-hour time scale. This annealing process is the object of the present study.

We will begin with a consideration of the experimental conditions necessary for and facilitating the application of ESR transient spectroscopy. This will be followed by a presentation of the experimental results obtained in the case of high-purity *a*-Si:H as well as of *a*-Si:N,H, *a*-Si:C,H, and *a*-Si:O,H alloys. Finally possible mechanisms underlying the annealing of the metastable dangling bonds in *a*-Si:H will be discussed.

EXPERIMENT

All ESR experiments were performed with a Varian E201 ESR system in the absorption mode, using 100-kHz field modulation. Normalized scans of the stable dangling-bond signal in an annealed *a*-Si:H sample and of the metastable dangling bonds in an illuminated sample are shown in Fig. 1(a). It is evident that the line shape of the stable and the metastable dangling bonds is, for any practical purposes, identical. This means that in the following the line-shape information provided by a conventional ESR spectrum is redundant, and the dangling-bond density N_S can be obtained directly from the peak-to-peak amplitude, A, of the derivative spectrum. More accurately, the relation between A and N_S is

$$A=CT^{-1}S(H_1,T_1)N_S\ . \tag{1}$$

Here C is a constant for a given sample determined by the sample volume and geometry, the spectrometer sensitivity, and the line-shape parameters. The factor T^{-1} reflects the Curie temperature dependence valid for the susceptibility of both the stable and metastable silicon dangling bonds at high temperatures, and the factor $S(H_1,T_1)$ describes the saturation behavior of the dangling-bond states as a function of microwave field H_1 and spin-lattice relaxation time, T_1. The H_1 dependence of the absorption signal, A, at $T=300$ K is shown in Fig. 1(b). Again, a nearly identical behavior for the stable and metastable dangling bonds is observed. This insures that Eq. (1) is valid independent of the stable or metastable nature of the spin states. Moreover, in the present case, the microwave field H_1 can be selected such that for all temperatures used ($300<T<500$ K), the temperature dependence of the saturation factor $S(H_1,T_1)$ to first order cancels the T^{-1} Curie temperature dependence of the ESR signal: with rising temperature, the decrease of T_1 leads to a

tion of the ESR absorption which compensates for the decrease in susceptibility over a limited temperature range. Thus, in the case of the metastable dangling bonds in *a*-Si:H, an extremely simple situation can be obtained, where the proportionality factor $CT^{-1}S(H_1,T_1)$ between dangling-bond spin density and ESR signal amplitude is independent of temperature. It should be noted, however, that in the general case the temperature dependence $T^{-1}S(H_1,T_1(T))$ of the ESR signal is not negligible, and thus has to be known for a correct analysis.

A primary requirement for the spectroscopically resolving ESR transients is the ability to measure the variations of the ESR spin density continuously over a wide time range. The most straightforward way to do this is by taking the usual ESR spectra at intervals determined by the minimum duration for a sweep through the dangling-bond resonance. This direct method leads to a time resolution of about 100 s, limited by the requirement to keep the speed of the static magnetic field sweep, dH_0/dt, much smaller than the ratio of the ESR linewidth and the time constant used for the signal detection, $\Delta H_{pp}/\tau$. If, however, as in the present case, the ESR line shape does not change during an annealing experiment, the line-shape information obtained by a complete sweep of the magnetic field across the paramagnetic resonance is no longer needed, and can be exchanged for a more accurate or faster information about the signal amplitude A. Experimentally, the spin density can then be determined by using the standard 100-kHz field modulation for the detection of the first derivative of the ESR absorption [Fig. 1(a)], with the static magnetic field H_0 fixed at the position of the maximum or the minimum in the derivative spectrum. The magnitude of this 100-kHz signal is then, according to Eq. (1), a measure of the spin density and can be recorded in a continuous way. Better signal-to-noise ratios and an improved stability against spectrometer drifts, however, can be obtained with the following double-modulation technique. As before, 100-kHz modulation is used to obtain the derivative ESR spectrum, but now H_0 is set to the zero-crossing position of the derivative. In addition, a second, much slower, field modulation with a peak-to-peak amplitude equal to the peak-to-peak linewidth ΔH_{pp} of the derivative spectrum is applied. As a result, the output signal of the ESR spectrometer varies between the minimum and maximum values of the derivative spectrum synchronously with the second modulation field, and the desired continuous spin-density information can be extracted from the ac output of the ESR spectrometer by lock-in amplification. All experimental data shown in the following were measured with this double modulation technique, using a frequency of 10 Hz for the additional field modulation and a time constant of 10 s for the lock-in amplifier.

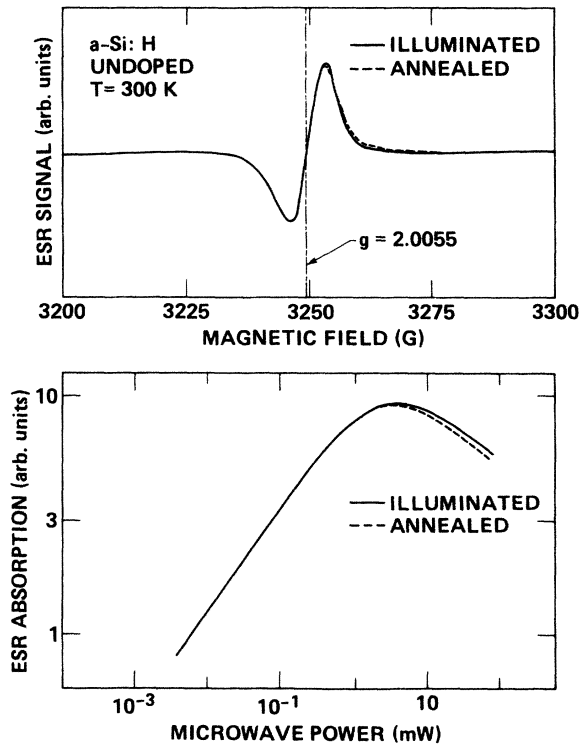

FIG. 1. (a) Normalized derivative ESR absorption spectra of the silicon dangling-bond resonance ($g=2.0055$) in undoped hydrogenated amorphous silicon in the annealed state (dashed curve) and the light-soaked state (solid curve). (b) Saturation of the ESR microwave absorption for the annealed (dashed curve) and the illuminated state (solid curve).

The spin density and the annealing temperature were monitored continuously with a stripchart recorder and an on-line computer for subsequent analysis. The temperature was set between 300 and 500 K with a nitrogen flow cryostat and was measured close to the sample with a thermocouple. The typical temperature stability during an annealing experiment is ± 1 K.

All samples used in this study were deposited on Corning 7059 substrates (5×10 mm) by rf glow discharge of silane in an ultra high vacuum (UHV) reactor. Details of the deposition system are described elsewhere.[5] The deposition conditions are 100 sccm (cubic centimeters per minute at standard temperature and pressure) silane flow rate, 2-W rf power, and 230°C substrate temperature. Film thicknesses lie between 1 and 3 μm. The composition of the films was determined by secondary-ion-mass spectroscopy (SIMS) analysis. The typical impurity concentrations of films deposited in the UHV reactor are $[O]\approx 2\times 10^{18}$ cm^{-3}, $[C]\approx 4\times 10^{17}$ cm^{-3}, $[N]\approx 5\times 10^{16}$ cm^{-3}. Higher concentrations of these impurities were achieved by controlled additions of, e.g., NH_3 or ultrapure O_2. Metastable defects were created by 16-hour illumination with white light (300 mW/cm^2).

RESULTS

An example for the decay curves obtained in the annealing experiments of metastable dangling bonds is shown in Fig. 2. After the second field modulation is turned on with the sample still at room temperature, the ESR transient signal rises at a rate determined by the lock-in time constant to the high initial level corresponding to the high defect density created during prolonged illumination. This signal is recorded for some time to establish the starting defect density, $N(0)$, with sufficient

accuracy. Then, the temperature is raised to the desired annealing temperature, e.g., $T_A = 120\,^{\circ}\mathrm{C}$ in the case of Fig. 2. This requires typically 5 min, during which the ESR transient signal already starts to decay because of the annealing of the dangling bonds. However, this transient region comprises only about 10% of the total decay and moreover, can be included in the final result by using the time-dependent rate analysis as developed in the preceding paper.[1] On the time scale shown in Fig. 2, temperature equilibration occurs almost immediately, and the decay of the ESR signal is governed only by the microscopic properties of the metastable dangling bonds. This decay depends in a roughly logarithmic way on annealing time, so that the decay rate at a constant temperature finally reaches a regime in which the annealing process has nearly stopped on a linear time scale. For the 120°C anneal in Fig. 2 this occurs after about 4 hours. For the annealing of the remaining metastable dangling bonds with a much slower decay rate, it is advantageous to increase the annealing temperature. In the example shown in Fig. 2, the temperature is raised from 120 to 170°C. The remaining metastable dangling bonds then anneal with a rate similar to the initial decay at 120°C. After a total annealing time of 14 hours, the ESR signal has reached the level given by the density of stable dangling bonds plus any signal due to background absorption. This level defines the asymptotic ESR signal, $N(\infty)$. For the following analysis it is imperative to determine $N(\infty)$ as accurately as possible, since the experimental quantity of interest, i.e., the light-induced metastable spin density

$$N_{\mathrm{ind}}(t) = N(t) - N(\infty)\,, \tag{2}$$

depends critically on the right choice of $N(\infty)$, especially in the long-time limit when $N(t) \approx N(\infty)$.

The application of the ESR transient analysis as described in Ref. 1 requires a monomolecular annealing kinetics,

$$\frac{dN_{\mathrm{ind}}(t)}{dt} = -RN_{\mathrm{ind}}(t) \tag{3}$$

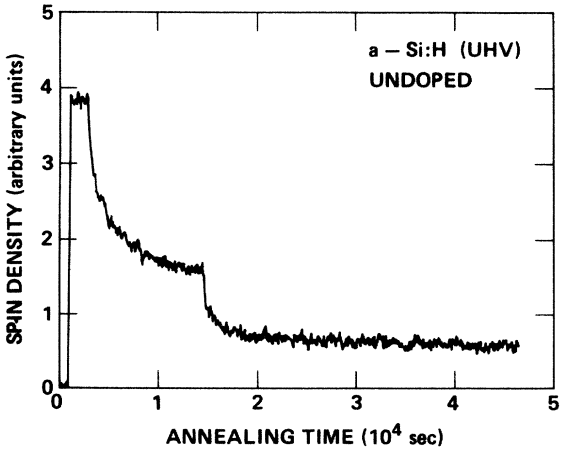

FIG. 2. Decay of the dangling-bond absorption as a function of annealing time for a 120–170°C annealing sequence. The decay curve was obtained with the double modulation technique described in the text.

in which the annealing of a metastable dangling bond occurs statistically independent of all the other metastable defects. Other possible annealing mechanisms involve higher-order kinetics,

$$\frac{dN_{\mathrm{ind}}(t)}{dt} = -RN_{\mathrm{ind}}^{m}(t), \quad m \geq 2\,. \tag{4}$$

For example, a bimolecular kinetics [Eq. (4) with $m=2$] has been proposed for the present case of metastable dangling bonds in a-Si:H by Lee *et al.*[6] Experimentally, the kinetic behaviors described by Eqs. (3) and (4) can be distinguished by an examination of the annealing decay for different initial spin densities, $N_{\mathrm{ind}}(0)$. In the case of Eq. (3), the decay can be transformed into the normalized form

$$\frac{dn}{dt} = -Rn \quad \text{with } n = N_{\mathrm{ind}}(t)/N_{\mathrm{ind}}(0)\,. \tag{3'}$$

In this normalized form, the observed decay is independent of the initial density of metastable spins, $N_{\mathrm{ind}}(0)$. In contrast, if the decay is given by Eq. (4), such a normalization is not possible. The decay for smaller initial densities $N_{\mathrm{ind}}(0)$ will always be slower, since the probability for processes involving the simultaneous reaction of more than one species depends on the density of these species.

Figure 3 shows that, for the metastable dangling bonds in a-Si:H, the monomolecular mechanism is consistent with the experimental results. The decay of $n = N_{\mathrm{ind}}(t)/N_{\mathrm{ind}}(0)$ has been measured for two initial defect densities varying by a factor of 4, $N_{\mathrm{ind}}(0) = 3\times10^{16}\ \mathrm{cm}^{-3}$ and $N_{\mathrm{ind}}(0) = 1.1\times10^{17}\ \mathrm{cm}^{-3}$, and the same decay curve is found in both cases. For a bimolecular annealing mechanism, the decay for the smaller initial defect density, $N_{\mathrm{ind}}(0) = 3\times10^{16}\ \mathrm{cm}^{-3}$, would have followed the dashed line in Fig. 3. This is clearly not the case.

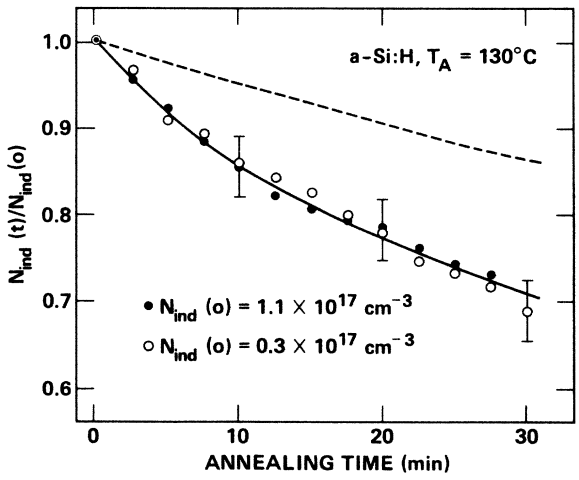

FIG. 3. Normalized metastable defect density. $N_{\mathrm{ind}}(t)/N_{\mathrm{ind}}(0)$, as a function of annealing time for two different initial densities: $N_{\mathrm{ind}}(0) = 3\times10^{16}$ and $1.1\times10^{17}\ \mathrm{cm}^{-3}$. The dashed curve shows the expected decay in the case of the lower $N_{\mathrm{ind}}(0)$ value and a bimolecular annealing mechanism. The stable spin density after complete annealing is $7\times10^{15}\ \mathrm{cm}^{-3}$.

Consequently, we may conclude that the annealing of the metastable spins follows a monomolecular mechanism, and the ESR transient analysis given in Ref. 1 can be applied to the present problem. We will proceed by writing the annealing rate R in Eq. (3) as

$$R=\nu_0\exp(-E_a/kT_A)\,, \tag{5}$$

i.e., as a thermally activated quantity with an activation energy E_a for the annealing transition, and an attempt-to-anneal frequency, ν_0. It should be mentioned that no direct experimental evidence exists for the validity of Eq. (5), but on the other hand, all microscopic models proposed so far for the metastable dangling-bond states as well as the strong temperature dependence of the annealing process are certainly consistent with an annealing rate according to Eq. (5). If one accepts Eqs. (3) and (5) as the relations describing the annealing of the metastable dangling-bond states, then the fact that no simple exponential dependence of $N_{\rm ind}$ on the annealing time t or temperature T_A is observed, suggests the existence of a distribution of the two parameters E_A and/or ν_0 governing the decay. The aim of the ESR transient analysis, then, is to extract these distributions from the annealing curves. This can be done by plotting the normalized metastable defect density $N_{\rm ind}(t)/N_{\rm ind}(0)$ as a function of $kT_A\ln(\nu_0 t)$. Then the correct value of ν_0 can be determined by requiring that annealing curves obtained at different annealing temperatures T_A overlap to yield a unique decay curve in $kT_A\ln(\nu_0 t)$ (see Fig. 4). The underlying distribution of activation energies E_A can be derived from this unique curve by taking its derivative with respect to $kT_A\ln(\nu_0 t)$. A more-detailed discussion of how the prefactor ν_0 and the distribution $N(E_a)$ of activation energies are determined from the decay curves is given in Ref. 1.

The results of the transient analysis for the case of a-Si:H deposited in an UHV reactor are shown in Fig. 5. For newly deposited samples, a prefactor of $\nu_0=10^{10}\ \mathrm{s}^{-1}$ was determined from previous decays versus annealing energies (Ref. 3) and a normalized spectrum according to Fig. 5(a) is obtained from the data. The annealing activation energies range from 0.9 to 1.3 eV, with the center of the distribution at 1.1 eV. Because the width of the spectral features in Fig. 5 is greater than $2.7kT$, no improvement over Eq. (9) of Ref. 1 can be obtained using iterative deconvolution [Eq. (10), Ref. 1] or inversion of the Laplace transform. The three-peak structure appearing in the distribution is reproducible for different runs on the same sample as well as from sample to sample, indicating that the metastable dangling bonds could be a combination of three subpopulations with different activation energies. Some irreversible changes or aging effects occur when the same sample is subjected to a large number of illumination-annealing cycles. This is shown in Fig. 5(b).

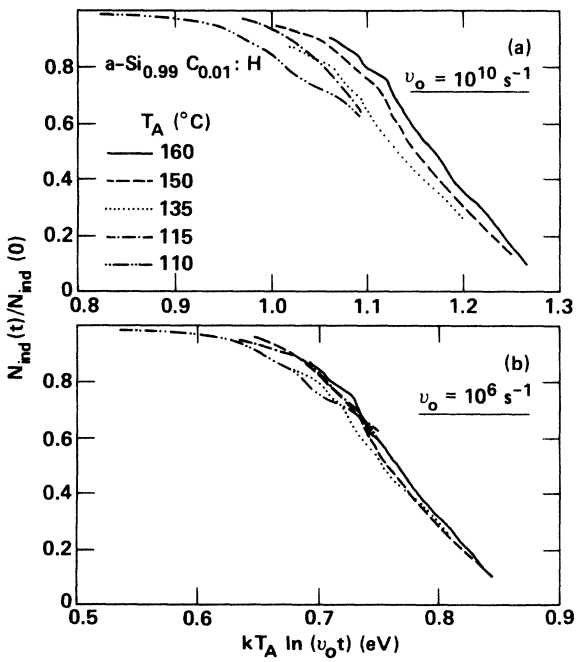

FIG. 4. Normalized decay curves for the metastable defects in a-Si:C,H at various annealing temperatures, T_A, plotted against the kinetic parameter, $kT_A\ln(\nu_0 t)$. (a) $\nu_0=10^{10}\ \mathrm{s}^{-1}$; (b) $\nu_0=10^{6}\ \mathrm{s}^{-1}$. Note the expanded scale in (b).

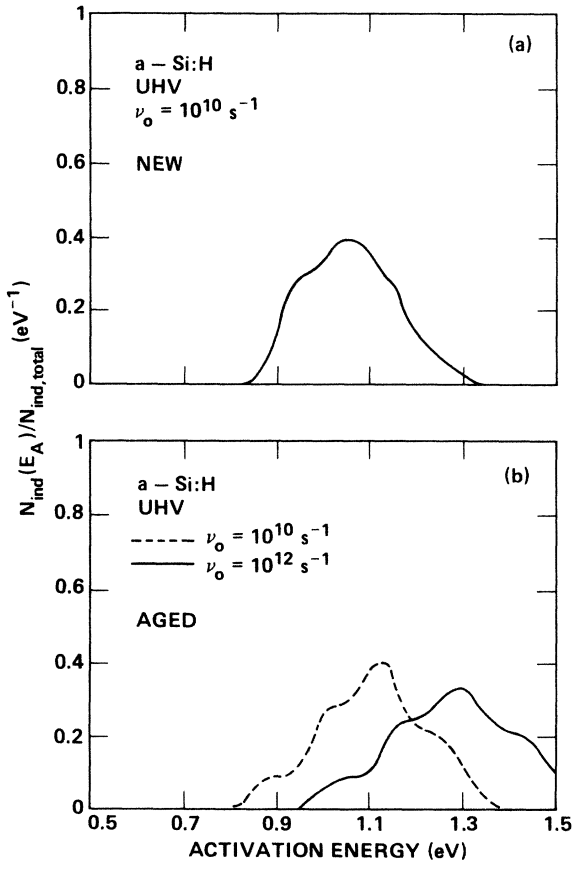

FIG. 5. Normalized distribution of annealing activation energies E_A in the case of a-Si:H deposited in a UHV reactor. The prefactor was obtained from data presented in Ref. 3. (a) Distribution in a newly deposited sample. (b) Distribution after a large number of illumination-annealing cycles plotted for two different prefactors, $\nu_0=10^{10}\ \mathrm{s}^{-1}$ (dashed curve) and $\nu_0=10^{12}\ \mathrm{s}^{-1}$ (solid curve).

If one first assumes a similar prefactor, i.e., $\nu_0 = 10^{10}$ s^{-1}, as for the new samples, an activation energy distribution as described by the dashed curve follows from the experiment. Compared to the distribution in Fig. 5(a), the main difference is that the multiple-peak structure becomes better resolved, accompanied by a slight broadening of the distribution and the appearance of an additional shoulder at the low-energy end. However, a more-detailed investigation of the annealing temperature dependence shows that the attempt prefactor ν_0 increases to a value of about 10^{12} s^{-1}. Hence, the energy distribution shifts to higher energies by about 0.2 eV, as indicated by the solid curve in Fig. 5(b). In the absence of a detailed microscopic model for the Staebler-Wronski effect, the origin of this shift to higher energy is not known. One possible explanation may be that the lower-energy defects have a certain probability of becoming more stable higher-energy defects during Staebler-Wronski cycles. The defect distribution would then drift to higher energies as the number of cycles increases.

The data presented in Fig. 5 shows that ESR decays can be used to obtain additional spectroscopic information about defects that otherwise seem identical. Even though the metastable dangling bonds in *a*-Si:H have identical ESR properties, their annealing energies are distributed over a range corresponding to about 20% of the entire mobility gap. Determining this distribution will be especially valuable for any detailed microscopic understanding of the metastable changes in *a*-Si:H, and we will come back to this question in the Discussion section below. Before doing so, however, we would like to demonstrate the spectroscopic capability of ESR transient analysis in the cases of *a*-Si:H samples with significant contents of common impurities like carbon, nitrogen, and oxygen. For all of these impurities, differences in the magnitude or the kinetic behavior of the light-induced metastable changes have been reported for impurity levels in excess of approximately 10^{20} cm^{-3}.[7-10] Despite of all these differences, the ESR spectra of the metastable defects observed in the impurity-rich samples are usually indistinguishable from those obtained for the metastable dangling bonds in pure *a*-Si:H. In these cases, therefore, the additional spectroscopic information provided by ESR transient analysis can lead to further insight into the microscopic origin of the metastable defects.

The first example to be discussed is that of amorphous silicon containing small amounts of carbon, *a*-Si_xC_{1-x}:H. Carbon is always introduced unintentionally into *a*-Si:H with concentrations between 10^{18} and 10^{20} cm^{-3}, e.g., because of hydrocarbons backstreaming from vacuum systems into the glow-discharge reactor. For carbon contents below 10^{20} cm^{-3}, usually no changes in the light-induced metastabilities of *a*-Si:H are observable. At higher concentrations, however, Crandall *et al.* have shown that, e.g., the degradation behavior of solar cells using *a*-Si_xC_{1-x}:H layers is altered considerably.[8] In the following, we will compare the ESR transient spectrum of an amorphous silicon sample containing about 1 at. % of carbon with that of ultrapure *a*-Si:H with at least 2 orders of magnitude less carbon in the solid phase. Compared to the ultrapure case as shown in Fig. 5, two significant differences occur with the introduction of carbon. First, the temperature dependence of the annealing decay curves shows that the annealing prefactor, ν_0, drops from the value 10^{10} s^{-1} found in pure *a*-Si:H, to the lower value of 10^6 s^{-1} in the carbon-rich sample. This is demonstrated in Fig. 4, where the normalized metastable defect density, $N_{\rm ind}(t)/N_{\rm ind}(0)$, is plotted as a function of the kinetic parameter, $kT_A \ln(\nu_0 t)$, for five different annealing temperatures T_A between 110 and 160 °C. In Fig. 5(a) the same attempt-to-anneal frequency as in pure *a*-Si:H, i.e., $\nu_0 = 10^{10}$ s^{-1}, has been assumed. It is evident that the existence of a unique decay curve required by Eq. (5) is not observed, indicating that a different ν_0 value has to be chosen.[1] In Fig. 4(b), the same decay curves are shown for the prefactor $\nu_0 = 10^6$ s^{-1}. Because of better overlap of the various decay curves for 10^6 s^{-1}, this represents a reasonably accurate value for ν_0 for the case of slight carbon contamination. [Note the change in the horizontal scale between Figs. 4(a) and 4(b).] The metastable defect distribution derived from the decay curve in Fig. 5(b) is depicted in Fig. 6. With respect to the transient spectrum obtained in pure *a*-Si:H [Fig. 4(a)], introduction of carbon at a 1% level leads to a shift of the spectrum to lower energies by about 0.4 eV. Moreover, the symmetric peak observed in pure *a*-Si:H is changed into a distribution of annealing activation energies which is approximately constant at energies $E_a > 0.7$ eV. The sharp cutoff occurring at $E_a \approx 0.85$ eV in the distribution in Fig. 6 is probably due to the fact the microscopic changes introduced by the enhanced carbon content prevent the formation of metastable defects with E_a larger than this cutoff energy. We will discuss this interesting point in the next section.

Before turning to this discussion, however, it is quite useful to have a look at the influence of two other common impurities in *a*-Si:H, oxygen and nitrogen. Both impurities have been linked to changes in the metastable properties of *a*-Si:H, when present in concentrations larger than 10^{20} cm^{-3},[7,10-12] whereas for concentrations lower than 10^{19} cm^{-3}, no influence of O or N on the light-induced degradation can be observed.[9] Therefore, we have determined the distributions for the metastable dangling bonds in two *a*-Si:H samples containing a signi-

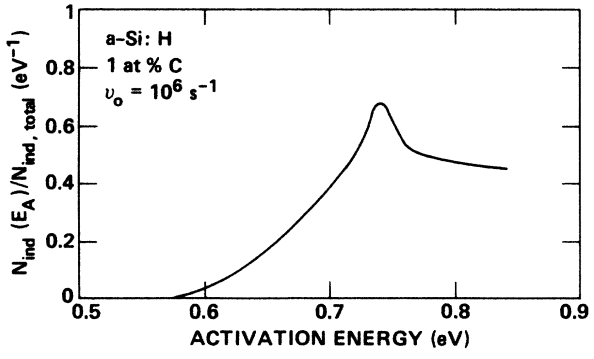

FIG. 6. Normalized distribution $N_{\rm ind}(E_A)/N_{\rm ind,total}$ for the annealing activation energies of metastable dangling bonds in *a*-Si:C,H (1 at. % C).

ficant number of either nitrogen impurities ([N] = 4 at.%) or oxygen impurities ([O] = 20 at.%). These spectra are shown in Figs. 7(b) and 7(c) with the transient spectrum of pure a-Si:H in Fig. 7(a) for comparison. Spectra for other impurity levels were not obtained.

Qualitatively, a similar influence of O or N on the metastable defect annealing energy distribution as in the case of carbon is observed. The symmetric E_a distribution of pure a-Si:H is replaced by a monotonously increasing spectrum with an abrupt high-energy cutoff near 1.3 eV for impurity-rich specimens. The low-energy end of the E_a distribution drops to 0.7 eV in both O- and N-rich a-Si:H. The attempt-to-anneal frequency, ν_0, for a-SiN_{1-x}:H is similar to that found in pure a-Si:H, $\nu_0 = 10^{10}\ s^{-1}$, whereas ν_0 drops to $10^8\ s^{-1}$ for oxygen-rich samples.

As in the case of pure a-Si:H, the impurity-rich samples also show some irreversible changes (aging) caused by repeated illumination-annealing cycles. For pure amorphous silicon samples, this led to a shift of the transient spectrum to higher energies (see Fig. 4), while the magnitude of the metastable changes remained unaffected. For a-Si:H samples with high nitrogen or oxygen contents, the reverse situation is observed. Repeated annealing-illumination cycles hardly change the annealing energy distribution of the metastable dangling bonds. Rather, the magnitude of the light-induced effect changes, observable as a decrease of the difference between the dangling-bond spin densities in the illuminated and the annealed state. This is shown in Figs. 8(a) and 8(b) for samples with relatively high nitrogen and oxygen contents, respectively. For both examples, the spin density observed in the an-

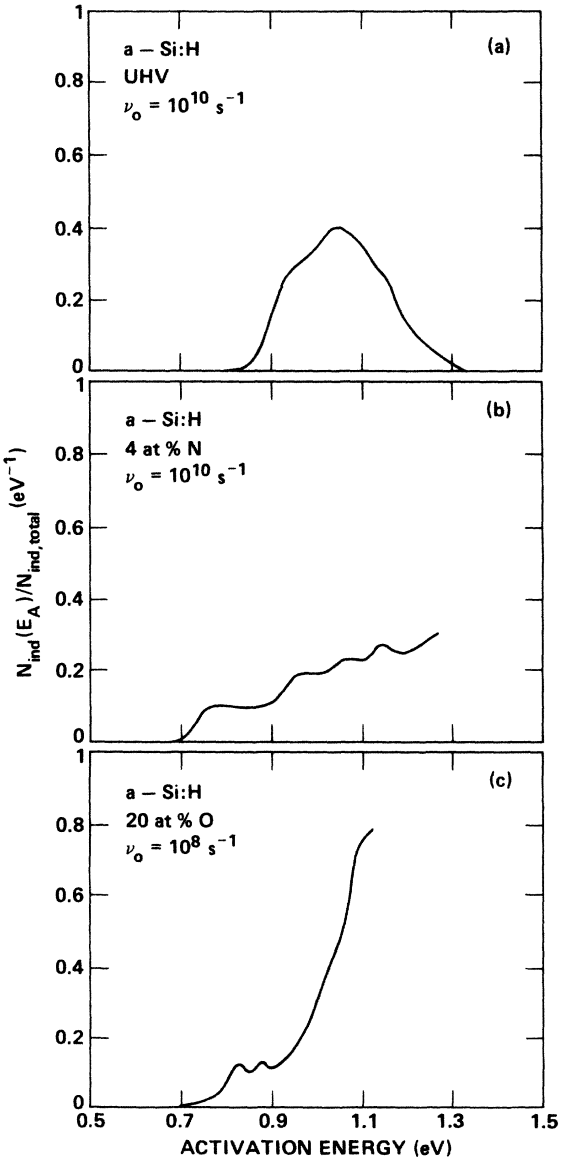

FIG. 7. Comparison of prefactors, ν_0, and annealing energy distributions in UHV-deposited (a) a-Si:H, (b) a-Si:N,H (4 at. % N), and (c) a-Si:O,H (20 at. % O).

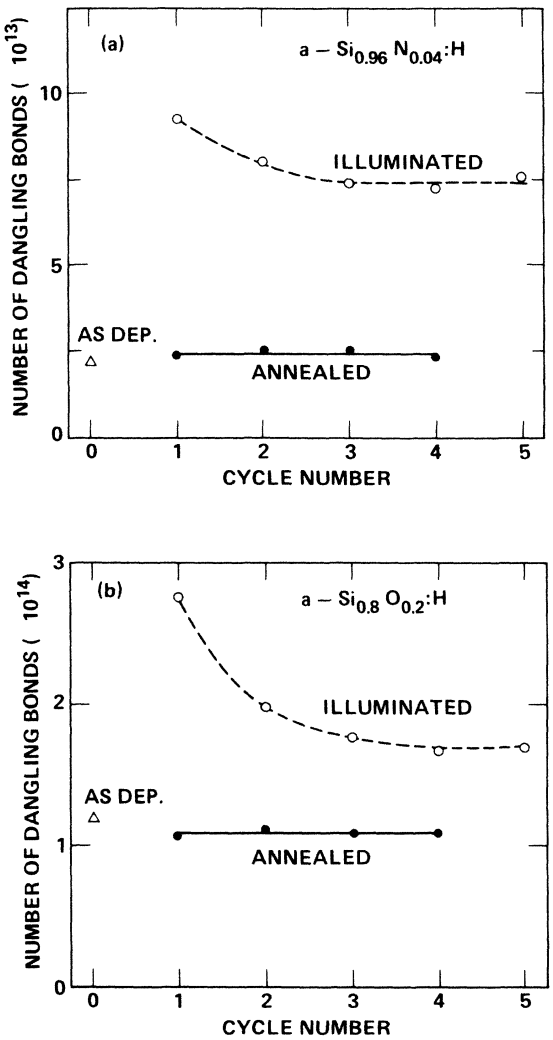

FIG. 8. Number of dangling bonds in the illuminated state (open circles) and the annealed state (solid circles) as a function of the illumination-annealing cycle number: (a) a-Si:N,H; (b) a-Si:O,H. The open triangles indicate the number of defects after deposition.

nealed state remains constant and is equal to the density measured immediately after deposition (open triangles). The defect density in the illuminated state, however, decreases by as much as 40% for subsequent cycles, but eventually reaches a regime with complete reversibility after three to four cycles.

DISCUSSION

The information provided by the ESR transient spectra for various cases in which metastable changes in the spin properties of hydrogenated amorphous silicon are observed, can be specified in terms of two quantities: (1) the spectral distribution $N(E_a)$ of metastable dangling bonds with an activation energy E_a for the transition into the thermodynamically stable ground state, and (2) the attempt frequency ν_0 for this transition. Phenomenologically, the interpretation of $N(E_a)$ and ν_0 as used in the ESR transient analysis is straightforward. Illumination creates metastable dangling bonds with an energy E_1, corresponding to a microscopic configuration q_1 (see Fig. 9). The metastable character of these states is due to the existence of an energy barrier $\{V_0=E_a;\Delta q=|q_1-q_0|\}$ separating the metastable state from the thermodynamically stable ground state, $E_0<E_1$, with a microscopic configuration q_0. In this picture, the distribution $N(E_a)$ of metastable dangling bonds with different annealing energies E_a is given by the product:

$$N(E_a)=B(E_a)p(E_a)\ . \tag{6}$$

Here $B(V_0=E_a)$ is the distribution of microscopic sites capable of undergoing the observed metastable changes characterized by their energy barrier height V_0 as defined in Fig. 9. The second factor, $p(E_a)$, is the probability that the metastable configuration, q_1, of a site with an energy barrier E_a becomes occupied during a given illumination procedure. Thus, $B(V_0)$ is determined by the microscopic properties of a given sample, for example, the concentration of various impurities, whereas $p(E_a)$ takes into account that even for the same sample different illumination conditions can lead to different distributions $N(E_a)$. Hence, previous results showing that metastable defects created by illumination at elevated sample temperatures are more difficult to anneal than defects created at room temperature, indicate a shift of $p(E_a)$ and therefore $N(E_a)$ to higher energies.[13] Also, it is obvious that $p(E_a)$ could depend on the photon energy used for the creation of the metastable defects.

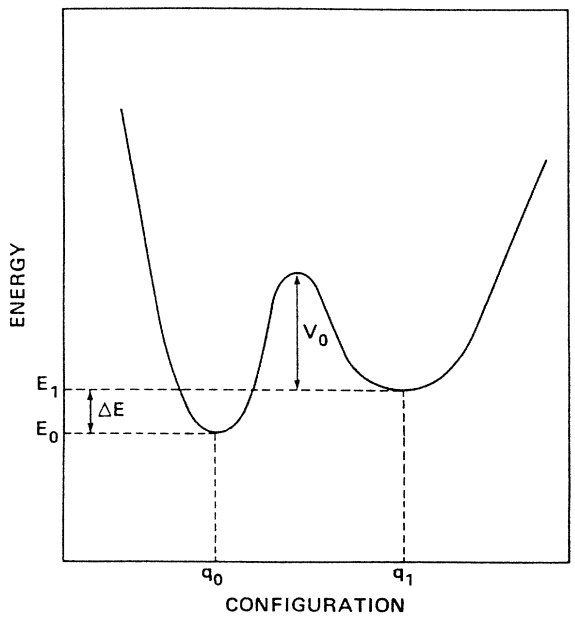

FIG. 9. Energy-configuration diagram for the light-induced dangling bonds in a-Si:H. q_1 represents the metastable state after light soaking, and q_0 the thermodynamically stable ground state.

For the experimental results presented in the preceding section, the main parameters controlling $p(E_a)$, i.e., illumination temperature, photon energy distribution, and sample absorptance, are always similar, so that the differences observed in the annealing energy distributions $N(E_a)$ must result from variations of the material related quantity $B(V_0)$. In this section we will propose possible annealing mechanisms compatible with our experimental data and with the mechanisms proposed earlier for the creation of the metastable defects. In addition, some comments on the role of impurities in the reversible changes can be made.

We begin with a discussion of the ESR transient spectrum observed in pure a-Si:H, as shown in Fig. 5(a). We have argued that in this case the creation of metastable dangling bonds by prolonged illumination is an effect intrinsic to a-Si:H,[3] implying that only silicon and hydrogen atoms should be involved in any microscopic explanation. The experimentally observed creation of additional Si dangling bonds shows then that either Si—Si or Si—H bonds have to be broken as a consequence of the illumination. The possibility of Si—H bond breaking can be excluded because of two reasons. First, the Si—H bonding energy is too high (3.5 eV) for bond breaking to occur at photon energies as low as 1.5 eV; and second, Si—H bond breaking should result in the formation of interstitial atomic hydrogen with its characteristic ESR spectrum, which is not observed. From this, it has been concluded that Si—Si bond breaking, especially the metastable breaking of weak Si—Si bonds known to exist in a-Si:H with densities up to 10^{18} cm^{-3}, is responsible for the light-induced metastable changes. A possible microscopic mechanism has been outlined in Ref. 3, and is shown in Fig. 10. According to this figure, the stable configuration q_0 in Fig. 9 is that of a weak Si—Si bond with a hydrogen atom bonded to one of the back bonds [Fig. 10(a)]. During optical excitation, a hole will be trapped preferentially in this weak bonding state. A nonradiative recombination of an optically excited electron into this hole state will then result in a sufficient vibrational excitation of the two Si atoms forming the weak bond to actually break this bond and to allow the back-bonded hydrogen atom to switch into the weak bond position with sufficient probability. Thus, the metastable state shown in Fig. 10(b) is created. We will now use the same microscopic model to discuss the annealing transition [Fig. 10(b)→10(a)]. The

first possible mechanism we would like to mention involves the thermal activation of the electron occupying the dangling-bond orbital in the back-bond position in Fig. 10(b) into a conduction-band state. As a result of such an excitation, the charge state of the corresponding silicon atom will change from neutral to $+e$, promoting the formation of sp^2 hybrid states for the remaining six electrons, rather than the usual sp^3 hybrids present in fully bonded silicon. This allows the hydrogen atom in Fig. 10 to swing back into a position intermediate between the positions shown in Figs. 10(a) and 10(b). When a thermally excited dangling-bond electron is recaptured by the positively charged complex, the transition probability out of the intermediate sp^2-hybridized state into the stable state [Fig. 10(a)] will be larger than the transition probability into the metastable state [Fig. 10(b)]. Therefore, as a result of the thermal excitation of a metastable dangling-bond electron, a net annealing transition [Fig. 10(b)$\rightarrow$10(a)] occurs. The $N(E_a)$ distribution observed experimentally is in good agreement with this annealing model. Since the rate limiting step for this annealing process is the thermal excitation of an electron from an occupied dangling-bond state below E_F into an empty conduction-band state near the mobility edge E_C, we can expect the distribution of metastable states to be negligible for $E_a \leq E_C - E_F \approx 0.8$ eV. Indeed, this agrees exactly with the experimental results shown in Fig. 5(a). For higher energies, $N(E_a)$ should be proportional to the metastable dangling-bond density of states N_{DB} at $E = E_C - E_a$:

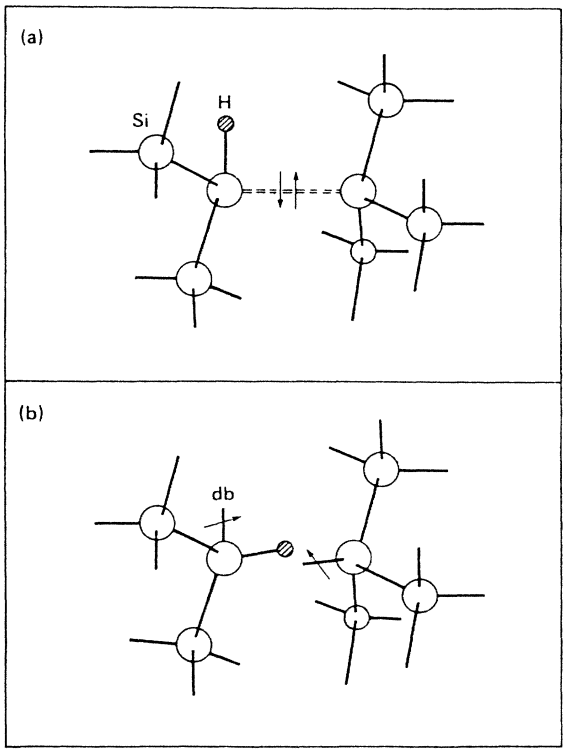

FIG. 10. One possible microscopic realization of the diagram in Fig. 9. (a) Stable state; (b) metastable state. See text for details.

$$N(E_a) \propto N_{DB}(E = E_C - E_a) . \quad (7)$$

In other words, for the annealing model proposed above, the distribution of annealing activation energies is expected to follow directly the metastable dangling-bond density-of-states distribution. Unfortunately, the latter distribution is still the subject of considerable controversy, so that definite conclusions concerning the annealing mechanism of the metastable dangling bonds cannot be drawn. On the other hand, the $N(E_a)$ distribution shown in Fig. 5(a) is in excellent agreement with N_{DB} distributions derived from completely unrelated experiments for stable dangling bonds,[14] so that this model for the annealing of metastable defects in a-Si:H as described here, certainly warrants further investigation. The second model, capable of explaining the observed annealing energy distribution and compatible with a microscopic model as shown in Fig. 10, involves direct thermal excitation of the back-bonded hydrogen atom. If, for example, the wagging mode of this hydrogen atom is excited to a vibrational energy equal to the energy barrier height V_0 in Fig. 9, an annealing transition [Fig. 10(b)$\rightarrow$10(a)] will become energetically possible. In this model, the distribution $N(E_a)$ of activation energies for the annealing step results from changes in the microscopic bonding environment of the hydrogen atom involved in the transition.

At this point it is not yet possible to argue more conclusively for any microscopic details of the annealing mechanism. Even such basic questions as to whether hydrogen is directly involved in the reversible process still remain to be decided experimentally. More experimental investigations are necessary, and we feel that ESR transient spectroscopy, because of its twofold spectroscopic capability, will be especially suited for these experiments. Useful extensions of the present study could involve an application of transient spectroscopy to metastable dangling bonds created at different illumination temperatures or with different photon energy distributions as well as an investigation of the metastable defects created by double carrier injection in p-i-n diodes.[15] Moreover, the annealing conditions could be altered to include bias illumination with visible or infrared light, in order to selectively introduce additional electronic or vibrational excitations.

In this investigation, we have chosen a different approach, namely to selectively change the sample properties by the incorporation of small amounts of impurities. This addresses the question whether the light-induced changes observed in a-Si:H are an intrinsic property of this material or whether they are caused by the presence of the impurities C, N, and/or O. As mentioned before, it is well documented that, for impurity concentrations above 10^{20} cm^{-3}, a direct correlation between the presence of these impurities and the magnitude of the metastable effects can be observed. Below this concentration, however, the density of light-induced defects is independent of the impurity content, and this fact has been used by the present authors to argue that in pure a-Si:H reversible changes constitute a phenomenon intrinsic to this material.[9] However, an often repeated counterargument has been that even the purest a-Si:H samples still contain significant amounts of impurities when compared to the den-

sity of metastable dangling bonds, which is typically 10^{17} cm^{-3}. Especially oxygen is known to exist in *a*-Si:H with concentrations at least 10 times higher than this defect density. The experimental results presented in the preceding section [cf. the transient spectra shown in Figs. 5(a), 6, and 7] demonstrate that in the impurity-enhanced regime ([C],[O],[N] $> 10^{20}$ cm^{-3}) each impurity leads to a specific spectral distribution of the metastable dangling bonds. Moreover, each of these distributions is characteristically different from what is observed in pure *a*-Si:H. This lends further support to our earlier conjecture about the intrinsic nature of the metastable changes in *a*-Si:H. If, for example, the metastable defects always were linked to the presence of an oxygen atom, one would instead expect similar ESR transient spectra for a wide range of oxygen content, as long as the oxygen-related centers still can be regarded as a dilute system.

On the other hand, it is easy to see how above a critical concentration of $\approx 10^{20}$ cm^{-3} the presence of impurities like oxygen, nitrogen, or carbon can change not only the magnitude of the observed light-induced changes, but also the spectral distribution of the metastable defects involved. It is known that these impurities lead to an increase of weak bonds in the band tails due to the increased bonding disorder,[16–18] which could explain the enhanced probability of metastable defect formation in the models outlined above. In addition, theoretical calculations predict a strong influence of these impurities on the energetic position of the dangling-bond states in the mobility gap.[19] When one of the Si atoms bonded to the central atom with the dangling-bond orbital is replaced by a C, N, or O atom, the energy of this dangling bond is raised relatively to the dangling-bond energy in pure *a*-Si:H. This happens because C, N, and O have a higher electronegativity than Si, leading to an admixture of antibonding character to the nonbonding dangling-bond wave function. Since the band-gap energy, E_g, is to first order unaffected by the incorporation of C, N, or O in the atomic percent level, the net effect of these impurities as far as dangling-bond states are concerned, is a broadening of the dangling-bond energy distribution in the mobility gap and a net shift towards the conduction-band mobility edge. This would provide one possible explanation for the observed changes in the ESR transient spectra upon impurity incorporation. If, as discussed above, the rate-limiting step for the annealing transition is the thermal activation of a metastable dangling-bond electron into the conduction band, the spectra should reflect the changes caused in the dangling-bond distribution by the presence of the impurity atoms.

However, some words of caution seem appropriate here. Too little is known about the microscopic origins of the light-induced changes in general, and the same is true for the detailed understanding of how impurities affect the structure or structural changes in *a*-Si:H. In this sense, the microscopic mechanisms for the annealing of metastable dangling bonds as discussed here should be regarded as working models, and not as definitive. Obviously, more experimental work is needed to sort out which parameters effect the annealing of metastable defects in what way, before any definitive explanations can be given. In addition, some theoretical calculations would be highly desirable, in order to test proposed models for their compatibility with the experimental data.

We would like to end this discussion by noting a rather peculiar property of the annealing kinetics. In Fig. 11, the logarithm of the prefactor ν_0 obtained by the ESR transient analysis has been plotted as a function of the activation energy E_a obtained through the same analysis. The crosses in Fig. 11 represent the values derived in this investigation, the length of the horizontal bars indicating the width of the distribution $N(E_a)$, and the vertical bars indicating probable errors in the determination of ν_0. The other data points in this figure were taken from earlier investigations of the annealing kinetics in *a*-Si:H and *a*-Si:C,H, which however, did neglect the existence of an energy distribution, $N(E_a)$ in their analysis. A strong correlation between ν_0 and E_a according to

$$\nu_0 = \nu_{00} \exp(E_a / E_0) \tag{8}$$

with $\nu_{00} \approx 1\ s^{-1}$ and $E_0 \approx 48$ meV ($\approx kT_0$ with $T_0 = 600$ K) is evident. A similar relation between the prefactors and the activation energies of thermally activated quantities is known as the Meyer-Neldel rule and is valid for a large number of amorphous semiconductors.[20] In the case of the amorphous silicon, the Meyer-Neldel rule takes the specific form

$$\sigma_0 = \sigma_{00} \exp(E_a / E_0') \ . \tag{9}$$

Here, σ_0 and E_a are the parameters characterizing the dark conductivity,

$$\sigma(T) = \sigma_0 \exp(-E_a / kT) \ , \tag{10}$$

and common values for σ_{00} and E_0' are $\sigma_{00} \approx 0.1$–$1\ (\Omega\,cm)^{-1}$ and $E_0' \approx 25$–50 meV, respectively.[21,22] The dark conductivity and the annealing kinetics in *a*-Si:H, therefore, show nearly identical dependences of the logarithm of the exponential prefactor on the activa-

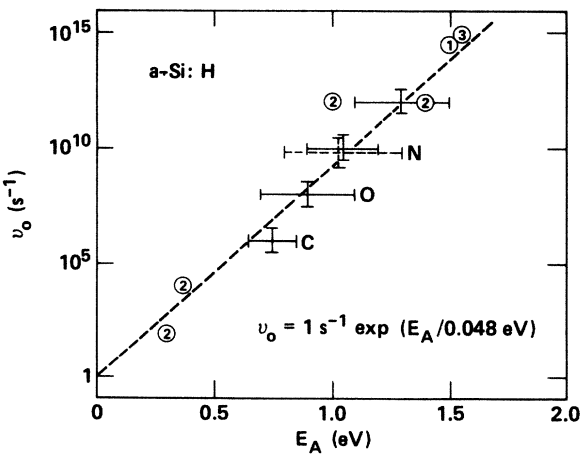

FIG. 11. Correlation between the attempt prefactor ν_0 and the annealing activation energy E_A in undoped *a*-Si:H. Crosses represent the distributions deduced from the present study, data points represent published results [(1) Ref. 23, (2) Ref. 8, (3) Ref. 24].

tion energy E_a'. Again, this might indicate that the same rate-limiting step, namely the thermal excitation of dangling-bond electrons into the conduction band, determines the conductivity and the annealing rate. Another possibility is, of course, that there are more general properties of amorphous silicon, like long-range potential fluctuations, which lead to Eq. (8) for the annealing of metastable dangling bonds and Eq. (9) for the conductivity in a similar way. An answer to this interesting question will require more experimental work, and ESR transient analysis should have further useful applications here.

CONCLUSIONS

We have applied a detailed analysis of ESR transients to the annealing process of metastable dangling bonds created by prolonged illumination in a-Si:H. The annealing of these metastable defects has been shown to obey a monomolecular reaction, characterized by an attempt frequency ν_0 and a distribution $N(E_a)$ of thermal activation energies. ν_0 and $N(E_a)$ have been measured for pure a-Si:H and for samples containing 1—10 at. % nitrogen, oxygen, and carbon. The incorporation of these impurities leads to $N(E_a)$ distribution that are significantly different from the spectrum observed in pure a-Si:H. This provides further evidence for the intrinsic nature of the metastable centers in pure material. Samples with N and O concentrations of the order of 10 at. % show significant irreversible changes (aging) between consecutive annealing-illuminations cycles. Definitive microscopic explanations for the annealing mechanisms cannot be given at this point, but a process based on the thermal excitation of metastable dangling-bond electrons seems to be consistent with the limited experimental data available. Finally, an interesting correlation between the attempt frequency ν_0 and the average activation energy E_a is presented. This correlation is found to be analogous to a similar phenomenon for the conductivity in a-Si:H known as the Meyer-Neldel rule.

ACKNOWLEDGMENTS

We are grateful to R. Thompson and A. J. Smith for their help with the sample preparation. This work was supported by the Solar Energy Research Institute (Golden, Colorado) under Contract No. XB-5-04067-1.

[1]W. B. Jackson, M. Stutzmann, and C. C. Tsai, Phys. Rev. B **34**, 54 (1986) (preceding paper).
[2]M. Stutzmann, W. B. Jackson, and C. C. Tsai, Appl. Phys. Lett. **45**, 1075 (1984).
[3]M. Stutzmann, W. B. Jackson, and C. C. Tsai, Phys. Rev. B **32**, 23 (1985).
[4]M. Stutzmann, Appl. Phys. Lett. **47**, 21 (1985).
[5]C. C. Tsai, J. C. Knights, R. A. Lujan, B. Wacker, B. L. Stafford, and M. J. Thompson, J. Non-Cryst. Solids **59/60**, 731 (1984).
[6]C. Lee, W. D. Ohlsen, P. C. Taylor, H. S. Ullal, and G. P. Ceasar, Phys. Rev. B **31**, 700 (1985).
[7]R. S. Crandall, Phys. Rev. B **24**, 7457 (1981).
[8]R. S. Crandall, D. E. Carlson, A. Catalano, and H. A. Weakliem, Appl. Phys. Lett. **44**, 200 (1984).
[9]C. C. Tsai, M. Stutzmann, and W. B. Jackson, in *Optical Effects in Amorphous Semiconductors,* proceedings of the International Topical Conference on Optical Effects in Amorphous Semiconductors held in Snowbird, Utah, 1984, edited by P. C. Taylor and S. G. Bishop (AIP, New York, 1984), p. 242.
[10]D. E. Carlson, A. Catalano, R. V. D'Aiello, C. R. Dickson, and R. S. Oswald, Ref. 9, p. 234.
[11]N. Nakamura, S. Tsuda, T. Takahama, M. Nishikuni, K. Watanabe, M. Ohnishi, and Y. Kuwano, Ref. 9, p. 303.
[12]A. Morimoto, H. Yokomichi, T. Atoji, M. Kumeda, I. Watanabe, and T. Shimizu, Ref. 9, p. 221.
[13]S. Guha, C.-Y. Huang, S. J. Hudgens, and J. S. Payson, J. Non-Cryst. Solids **66**, 65 (1984).
[14]N. M. Johnson and D. K. Biegelsen, Phys. Rev. **B 31**, 4066 (1985).
[15]W. den Boer, J. J. Geerts, M. Ondris, and H. M. Wentinck. J. Non-Cryst. Solids **66**, 363 (1984).
[16]E. Holzenkämpfer, F.-W. Richter, J. Stuke, and U. Voget-Crote, J. Non-Cryst. Solids **32**, 327 (1979).
[17]J. C. Knights, R. A. Street, and G. Lucovsky, J. Non-Cryst. Solids **35& 36**, 279 (1980).
[18]R. Carius, K. Jahn, W. Siebert, and W. Fuhs, International Conference on Luminescence (Madison, 1984) (unpublished).
[19]G. Lucovsky and S. Y. Lin, Ref. 9, p. 55.
[20]W. Meyer and H. Neldel, Z. Tech. Phys. **18**, 588 (1937).
[21]H. Fritzsche, Sol. Energy Mat. **3**, 447 (1980).
[22]P. Irsigler, D. Wagner, and D. J. Dunstan, J. Phys. C **16**, 6605 (1983).
[23]D. L. Staebler and C. R. Wronski, Appl. Phys. Lett. **31**, 292 (1977).
[24]D. Wagner and P. Irsigler, Appl. Phys. A **35**, 9 (1984).

Energy and Z_2 dependences of energy straggling for fast proton beams passing through solids

Yoshiaki Kido
Toyota Central Research and Development Laboratories, Inc., 41-1, Aza Yokomichi, Oaza Nagakute, Nagakute-cho, Aichi-gun, Aichi-ken, 480-11, Japan
(Received 17 December 1985)

The energy and Z_2 (target atomic number) dependences of energy straggling for fast proton beams are investigated using nuclear resonance reactions of $^{19}F(p,\alpha\gamma)^{16}O$ and $^{27}Al(p,\gamma)^{28}Si$. The results are compared with theoretical predictions based on the free-electron models (of Bohr and of Vavilov) and the local-electron-density models (of Lindhard and Scharff and of Chu). Concerning both energy and Z_2 dependences, the experimental data agree well with Chu's prediction using the Hartree-Fock-Slater charge distributions of the target atoms.

I. INTRODUCTION

A fast ion that penetrates a medium loses its energy via a number of successive collisions. This leads to statistical fluctuations in the energy loss of the ion beam around its average value, i.e., energy straggling. The values of the energy straggling for light ions are important parameters for simulation of a Rutherford backscattering spectrum and an excitation spectrum for a nuclear resonance reaction in ion-beam analysis.[1,2]

In the high-energy region above several tens of keV/amu, electronic interactions dominate the slowing-down process of a fast ion beam. So far, two different theoretical approaches have been developed concerning electronic straggling. One derives an accurate energy distribution function by solving a transport equation. This approach originated from Landau's formalism[3] and was then extended by Vavilov[4] under the assumption that all the target electrons are free. Another calculates directly the full width at half maximum (FWHM) of the energy-loss distribution assuming it to be a Gaussian. In the high-energy limit where all the target electrons are considered free, Bohr[5] derived the simple expression given by

$$\Gamma_B^2=(32\ \ln 2)\pi Z_1^2 Z_2 e^4 N\Delta R\ , \tag{1}$$

where e is the electron charge, Z_1 and Z_2, the atomic numbers of the projectile and the target atoms, respectively, and $N\Delta R$ the target thickness (atoms/cm^2). Lindhard and Scharff[6] extended Bohr's treatment by considering the local electron density of the target atom. The reduced straggling is expressed by

$$\Gamma^2/\Gamma_B^2=\frac{1}{Z_2}\int_0^\infty 4\pi r^2\rho(r)\frac{\Gamma^2(\rho(r),v)}{\Gamma_B^2}dr\ , \tag{2}$$

where $\rho(r)$ denotes the electron density of the target atom, $\Gamma^2(\rho(r),v)$ the contribution from various parts of the electron cloud to the straggling. They proposed the simple asymptotic formula

$$\Gamma^2/\Gamma_B^2=\begin{cases}L(\chi)/2 & \text{for } \chi\lesssim 3\ ,\\ 1 & \text{for } \chi\gtrsim 3\ ,\end{cases} \tag{3}$$

where $L(\chi)=1.36\chi^{1/2}-0.016\chi^{3/2}$. Here, χ is a reduced energy variable defined by $\chi=v^2/(Z_2 v_0^2)$ (v is the ion velocity, and v_0 the Bohr velocity). Bonderup and Hvelplund[7] refined this model by using the electron charge density $\rho(r)$ calculated from the Lenz-Jensen model. Similar calculations based on the Hartree-Fock-Slater model were carried out by Chu.[8]

Up to now, several experimental results on electronic straggling have been reported.[9–14] However, there are large discrepancies not only between experimental data and theoretical predictions but also between different measurements. This is probably due to the target conditions such as texture and film nonuniformity, which yield additional contributions to the energy straggling. As experimental methods, the backscattering or transmission technique combined with solid-state detectors has been usually employed. In the transmission experiment, we must prepare self-supporting target foils smoothed out, and we frequently need backing foils to prevent their breakage. On the other hand, the backscattering spectrum includes the contributions from the incoming and outgoing paths in the target film. These situations cause inaccuracies in determining the straggling values. In addition, the energy resolution of solid-state detectors is only 10 keV at best. Thus, in order to get accurate straggling data, the transmission technique with a magnetic or electrostatic spectrometer is most desirable. So far, only a few reports on straggling measurements using this technique have been made for heavy ions (lithium, nitrogen, and neon) passing through solids[15,16] and for proton and helium in gases.[17]

In the present experiment, we employed a new technique using nuclear resonance reactions with narrow natural widths. The nuclear reactions of $^{19}F(p,\alpha\gamma)^{16}O$ and $^{27}Al(p,\gamma)^{28}Si$ were used for this purpose. This technique makes it easy to prepare a variety of thin and smooth target films and gives good energy resolution. The principle of this method is to derive the straggling width from the slope of the excitation spectrum of γ-ray yields for the Al or LiF substrate onto which a thin target film is deposited. In order to obtain accurate straggling values, the excitation spectrum is generated theoretically